Journal of Biological Inorganic Chemistry, 7 (3), 2002

IR-Spectroelectrochemical study of the binding of carbon monoxide to the active site of *Desulfovibrio fructosovorans* Ni-Fe hydrogenase

Antonio L. De Lacey (□) - Christian Stadler - Victor M. Fernandez

Instituto de Catalisis, CSIC, Campus Universidad Autonoma-Cantoblanco, Madrid 28049, Spain

E-mail: alopez@icp.csic.es

Phone: 34-915854813

Fax: 34-915854760

E. Claude Hatchikian

Bioenergetique et Ingenierie des Proteins, Institute de Biologie Structurale et Microbiologie, CNRS, Chemin Joseph Aiguier, 13402 Marseille, Cedex 20, France

Hua-Jun Fan - Shuhua Li - Michael B. Hall

Department of Chemistry, Texas A&M University, College Station, Texas 77843, USA

Abstract. The binding of carbon monoxide, a competitive inhibitor of many hydrogenases, to the active site of *Desulfovibrio fructosovorans* hydrogenase has been studied

by infrared spectroscopy in a spectroelectrochemical cell. Direct evidence has been obtained of what redox states of the enzyme can bind extrinsic CO. Redox states **A**, **B** and **SU** do not bind extrinsic CO, only after reductive activation of the hydrogenase can CO bind to the active site. Two states with bound extrinsic CO can be distinguished by FTIR. These two states are in redox equilibrium and are most probably due to different oxidation states of the proximal 4Fe4S cluster. Vibrational frequencies and theoretical quantum mechanics studies (DFT) of this process preclude the possibility of strong bonding of extrinsic CO to the Fe or Ni atoms of the active site. We propose that CO-inhibition is caused by weak interaction of the extrinsic ligand with the Ni atom, blocking electron and proton transfer at the active site. A calculated structure with a weakly bound extrinsic CO at Ni has relative CO frequencies in excellent agreement with the experimental ones.

Keywords. Metalloprotein- FTIR - spectroelectrochemistry - carbon monoxide – Density Functional Theory

Introduction

Hydrogenases are enzymes that catalyze the reversible oxidation of H_2 to protons (equation 1) in biological systems. As they are efficient catalysts of this simple chemical reaction, there is great interest in the relationship between structure and function and in their applications in bioenergetics and fuel production. Three different types of hydrogenases can be recognized taking into account their metal content: the first group includes those which have Fe as only metal in their structure [1], the second group have in addition one Ni atom [2, 3, 4], and finally a novel metal-free hydrogenase has recently been characterized [5].

$$H_2 \rightleftharpoons 2H^+ + 2e^- \qquad (1)$$

The first X-ray structure of a hydrogenase to be solved was that of the Ni-Fe hydrogenase from *Desulfovibrio gigas* in its oxidized inactive state [6]. The crystallographic analysis showed that the active site of the enzyme contains two metals, one of which is Ni.

The Ni atom has four cysteine ligands, two of which bridge with the second metal atom. Three FeS clusters form the putative electron transfer pathway between the active site and the protein surface. Two of them are 4Fe4S clusters, one proximal to the active site and the other distal. A 3Fe4S cluster is placed between them [6]. Later crystallographic data confirmed that the second metal of the active site is an Fe atom which binds three non-protein diatomic ligands, and that a putative oxygen species bridges both metal atoms [7]. The diatomic ligands are detected by infrared spectroscopy in the 1900-2100 cm^{-1} region. Infrared (IR) studies of C*hromatium vinosum* [8] and *D. gigas* [7] Ni-Fe hydrogenases showed that each redox state of the active site is defined by a set of three IR bands, one of which is an intense band at lower frequencies whereas the other two bands are less intense and appear at higher frequencies. These bands shift in frequency when the redox state of the enzyme's active site changes. Isotopic substitution of the Fe diatomic ligands allowed to identify them as one CO and two CN^- groups [9]. The most intense band is due to the stretching vibration of CO, whereas the other two bands are due to two coupled CN^- oscillators [10].

Electrochemically controlled titrations of the different redox states detected by IR spectroscopy of *D. gigas* hydrogenase allowed to identify the redox and acid-base equilibria that correlate them [11]. These IR states are named **A, B, C, SI**, **SU** and **R** (Figure 1). **A, B** and **C** states have also been detected by EPR spectroscopy in many Ni-Fe hydrogenases [12, 13, 14, 15, 16]. **A** corresponds to an oxidized inactive state which is also named "unready" enzyme because it only becomes catalytically functional after a long activation process under reductive conditions [17]. **B** is also an oxidized inactive state but it quickly becomes active upon reduction. For this reason it is also known as "ready" enzyme [17]. **C** corresponds to active enzyme and when illuminated at low temperature it dissociates a hydrogen species [13]. **SU**, **SI** and **R** are EPR-silent states. **R** and **SI** are thought to be involved in the catalytic cycle as well as **C** [7**,** 18, 19]. Two sets of IR bands are detected for the **SI** redox state, which have been named $\mathbf{SI_I}$ and $\mathbf{SI_{II}}$. These two forms are in acid-base equilibrium [11]. **SU** is

obtained by reduction of unready enzyme at low temperatures and it is a transient state during the activation process [11].

Carbon monoxide is a competitive inhibitor of most Ni-Fe hydrogenases [20, 21]. The EPR spectrum of active enzyme changes in the presence of CO [14, 22]. Photodissociation at low temperatures of this species and of **C** gives the same EPR spectrum (termed **L**) [22]. Thus, it was proven that CO binds to the **C** state. As the EPR signal of CO-inhibited hydrogenase disappears under 100 % CO atmosphere, it was proposed that an EPR-silent state also binds extrinsic CO [22]. More recently, CO binding to Ni-Fe hydrogenases was demonstrated by IR spectroscopy [23].

In this work we report an IR-spectroelectrochemical study of *D. fructosovorans* Ni-Fe hydrogenase, which has a structure very similar to that of *D. gigas* [24], under CO-saturating conditions. The goal was to obtain direct evidence of which redox states of the hydrogenase can bind extrinsic CO and to determine if this binding process blocks the oxidation/reduction at the active site. Our IR-spectroelectrochemical cell is well suited for this type of study for the following reasons: 1) All redox states of the enzyme can be detected by IR-spectroscopy, including those that have extrinsic CO bound to the active site. 2) The redox potential of the sample is controlled *in situ*. 3) Redox titrations are performed at the same temperature as the spectroscopic measurements.

Experimental Section

Desulfovibrio fructosovorans Ni-Fe hydrogenase was purified as described [15]. The hydrogenase samples were concentrated in Centricon-30 (Amicon) to 0.6-0.8 mM prior to the IR-spectroelectrochemical measurements. The infrared spectra were recorded in a Nicolet 860 Fourier-transform spectrometer, equipped with a MCT detector and a purge gas system for removal of CO_2 and H_2O (Whatman Inc.). The IR-spectroelectrochemical cell has been described by Moss *et al.* [25]. Redox equilibrium in the cell was reached 2-3 minutes

after a potential was applied (checked by monitoring *in situ* the visible spectra of methyl viologen reduced at the cell's working electrode). The cell pathlength was measured by visible absorption spectroscopy of 8 mM cytochrome c. An average value of 7.5 μm was measured from six different experiments. For each FTIR measurement 10 μl of enzyme solution in 100 mM buffer, 100 mM KCl and a mixture of redox mediators, 0.5 mM each, were added in the cell. The redox mediators used were as follows: indigo-tetrasulfonate (E'_0= -76 mV at pH 8.0, Aldrich), indigocarmine (E'_0= -163 mV at pH 8.0, Fluka), anthraquinone-1,5-disulfonic acid (E'_0= -234 mV at pH 8.0, ICN Pharmaceuticals), anthraquinone-2-sulfonate (E'_0= -277 mV at pH 8.0, Serva), benzyl viologen (E'_0= -358 mV at all pH, Sigma) and methyl viologen (E'_0= -449 mV at all pH, Sigma). When required, the hydrogenase samples were bubbled with CO (Air Liquide) through a rubber septum for 10 minutes in an ice bath. Then, the sample was transferred to the spectroelectrochemical cell in a glove box under CO atmosphere. All safety precautions were taken.[1] 99% ^{13}CO was supplied by Aldrich. The redox potential of the cell was controlled with a BAS CV-27 potentiostat and measured with a Fluke 77 multimeter. All redox potentials are given against the normal hydrogen electrode (NHE). The temperature of the cell was controlled with a Huber CC 230 thermostat. The IR spectra were averaged from 124 scans and the spectral resolution was 2 cm^{-1}. The spectra were blank-substracted and baseline corrected using OMNIC software from Nicolet. The areas of overlapping bands were calculated by Fourier deconvolution.

The reduction of the FeS clusters of the hydrogenase in the spectroelectrochemical cell was measured with a Uvikon 940 spectrophotometer (Kontron Instruments) at 420 nm [15]. EPR spectra were measured in a nitrogen finger at 77 K with a Bruker ER200D spectrometer working in the X-band. The frequency was 9.36 GHz and the microwave power was 20 mW.

DFT calculations on active site models were done with the Amsterdam density functional (ADF) program package [26, 27] using Slater-type orbitals and the ZORA (zeroth-order regular approximation) relativistic approach [28, 29]. The spin-restricted scalar

relativistic calculations employed the pure local density functional of Vosko *et al.* [30] and a double zeta basis set (triple zeta for the 3d shell of Fe and Ni) without polarization functions. All non-valence orbitals were treated within the frozen core approximation. The computational models are based on a crystal structure of the hydrogenase from the Ser499Ala mutant of *D. fructosovorans* [24] and include the guanido group of Arg470, which was kept fixed during the geometry optimization. Also the nitrogen atoms of the cyanides and the methyl groups of the four S-CH_3 fragments representing the cysteine ligands were kept fixed at their experimental position (Figure 2).

Additional DFT calculations were also done with Gaussian 98 [31], specifically with the Becke [32] three-parameter hybrid exchange functional and the Lee-Yang-Parr [33] correlation function (B3LYP). The model molecule used is $[(CO)(CN)_2Fe(\mu\text{-}SMe)_2Ni^{II}(SMe)(SHMe)]^-$ for $\mathbf{SI_{II}}$. The basis sets used for the Fe and Ni were described by Hay and Wadt with effective core potentials (LANL2DZ) [34, 35]; the outer p orbital in the LANL2DZ basis sets were replaced by an optimized split valence functions from Couty and Hall [36] and a f-type polarization functions were added to both metals [37]. The basis set for S is standard LANL2DZ augmented with a d-type polarization function.[38, 39] For the CO and CN ligands bonded to the Fe center, a 6-31G(d) basis set is used [40]. The hydrogen atom bonded to the terminal sulfur and the carbon atoms in SMe groups have 3-21G basis sets [41]. For those hydrogen atoms in methyl groups, a STO-3G basis set is used [42]. The protein backbone was not included in the modeling because of the time and cost. Frequency calculations at the same basis set and method are carried out not only to verify the minimum of the structure, but also to predict the CO stretching frequencies, which will be compared with the experimental values. All Gaussian calculations were performed at the Supercomputer Facility of Texas A&M University.

Results

Figure 3A shows the IR spectra of *D. fructosovorans* hydrogenase at different redox potentials before and after activation. Comparison of these spectra with those reported for *C. vinosum* [8] and *D. gigas* [7] hydrogenases allows identifying unambiguously the bands that correspond to each redox state of the enzyme. Table 1 compares the frequency values of the IR bands for each redox state of *D. fructosovorans* hydrogenase with those of *D. gigas* hydrogenase. Only slight differences are observed. Spectrum a of Figure 3A shows that the as isolated *D. fructosovorans* hydrogenase was a mixture of **A** and **B** forms. In agreement to our previous results [11], when we reduced the sample *in situ* at low temperature we saw a mixture of **SU** and the two **SI** forms (spectrum b**)**. After activation of the sample in the cell we observed only the **SI** states (spectrum c). As we decreased the redox potential we detected first the **C** state (spectrum d) and then two **R** states (spectrum e). As observed with the two **SI** states [11], these two **R** forms are probably in acid-base equilibrium because the intensity of the 1922 band increases relative to the 1938 band with the pH (data not shown). When we oxidized the activated sample we obtained the pure **B** state (spectrum f). Figure 3B shows the IR spectra obtained when the sample was saturated previously with CO. Spectrum a indicates that the extrinsic CO does not bind to the **A** and **B** states as the spectrum is identical to the one obtained in absence of CO. The reduced spectrum at low temperature (spectrum b) shows the bands of **SU** but not those of the **SI** states. Instead, 4 bands appeared at frequencies 1930, 2056, 2069 and 2083 cm^{-1}. These bands are very similar to the ones reported for the **SI-CO** state of *C. vinosum* hydrogenase, in which one of the bands was due to the extrinsic CO bound to the active site of the hydrogenase [23]. We conclude that **SU** does not bind extrinsic CO, whereas **SI** does. After activation of the hydrogenase only the four bands of the **SI-CO** state are observed (spectrum **c**). In spite of observing two sets of bands for the **SI** state, only one set of bands is observed for **SI-CO**. This is true for the pH range 6-9 (not shown). Thus, binding of extrinsic CO only stabilizes one of the acid-base equilibrium species of **SI**.

Reduction at -395 mV produces a shift of 1-3 cm^{-1} to lower frequencies of the four bands (spectrum d). We have named this new IR state **$(SI\text{-}CO)_{red}$.** Application of lower redox potentials caused the reduction to **R** of a small proportion of **$(SI\text{-}CO)_{red}$** (spectrum e). Therefore, the **$(SI\text{-}CO)_{red}$** state is mostly blocked to reduction. In addition, **SI-CO** is completely blocked to oxidation (spectrum f).

The **SI-CO** and **$(SI\text{-}CO)_{red}$** states are in redox equilibrium as shown in Figure 4. Fourier deconvolution of the overlapping bands at 1928 at 1931 cm^{-1} allows plotting the integrated intensity of each band *versus* the redox potential. Both redox titrations can be fitted to the Nernst equation for an one-electron redox process. A formal potential of -325 ±10 mV is obtained for this redox equilibrium by calculating the mean value of the two curves.

An experiment was done in which the CO-saturated hydrogenase was activated in the IR-spectroelectrochemical cell at a more negative redox potential than the one applied in Figure 3. Activation at -495 mV gives a spectrum (Figure 5A) in which there is a higher proportion of the **R** state than in spectrum e of Figure 3B. Oxidation of **R** in presence of CO gave only **$(SI\text{-}CO)_{red}$,** as observed in spectra B and C of Figure 5. No **C** state is detected at –395 mV. Therefore, we can be sure that we indeed had a saturating concentration of CO. This experiment was done at normal laboratory light and in the dark. No difference in the results was observed. We conclude from this experiment that the **R** state is stable in presence of CO whereas the **C** state is not. In presence of CO the **C** state evolves to the same species than that obtained by one-electron reduction of **SI-CO** (Figure 3B, spectrum d).

Figure 6A shows the IR spectrum recorded with a hydrogenase sample saturated with ^{13}CO and activated. Only one band shows an isotopic shift of its frequency compared with the CO-saturated sample (spectrum c of Figure 3B). This shift of 46 cm^{-1} is very close to the one expected (45 cm^{-1}) if we consider the diatomic ligand CO as a simple harmonic oscillator [43]. Similar results were found by Bagley *et al*. with *C. vinosum* hydrogenase [23]. Therefore, we can be sure that the 2056 cm^{-1} band of spectrum **c** of Figure 3B is due to the

stretching vibration of the extrinsic bound CO. Reduction of **SI-^{13}CO** to **(SI-^{13}CO)$_{red}$** causes shifts of the frequencies of the bands due to the intrinsic and extrinsic ligands in the same direction and of similar magnitude (Figure 6).[2]

The reduction of the Fe-S clusters of the CO-inhibited hydrogenase was followed placing the spectroelectrochemical cell in a UV/visible spectrometer and measuring the decrease of absorbance at 420 nm when negative reduction potentials were applied (in absence of redox dyes).[3] Figure 7 shows that 20% of the clusters are reduced between 0 and –225 mV. 80% of the clusters are reduced between –225 and –400 mV, the same redox potential step in which the shift of FTIR bands is observed from **SI-CO** to **(SI-CO)$_{red}$** (Figure 4). At lower redox potentials no further decrease of the absorbance took place. The measured global decrease is in agreement with the change of extinction coefficient of the three Fe-S clusters of *D. fructosovorans* hydrogenase upon reduction [15].

In order to ascertain if the shift observed in the FTIR bands of the CO-inhibited hydrogenase upon reduction was due to a change of the redox state of the active site Ni atom, a sample of the enzyme was activated under H_2, then put under CO atmosphere, and the FTIR and EPR spectra were recorded in parallel. The FTIR spectrum of the sample was the same as spectrum c of Figure 3B (**SI-CO)**. After addition of sodium dithionite the FTIR bands shifted to those of spectrum d of Figure 3B (**(SI-CO)$_{red}$**). However, the EPR spectra showed that the Ni atom remained EPR-silent.

DFT calculations on active site models with an additional CO ligand were done in order to help the interpretation of the experimental results of this work. We would like to note that the accuracy of the computational methods presented here has been extensively tested in other studies [44, 45, 46]. The important finding is that good agreement between calculated and experimental structural parameters can be expected. Although we cannot predict exact IR frequencies, comparison of calculated and experimental C-O bond lengths will allow for the discrimination of reasonable and unreasonable models of the two CO inhibited states.

An important general result of the computational study done with the ADF program (Table 2) is the inability of the extrinsic CO to bind as terminal ligand to the iron center. This is due to steric restrictions caused by the guanido group capping the active site, which has been included in the model (Figure 2). The only possible binding modes are thus a bridging CO between the two metal centers or a terminal CO at the Ni site. Table 2 reports calculated carbonyl bond lengths taken from eight optimized active site models that might be possible candidates for **SI-CO** or **(SI-CO)$_{red}$**. In all cases the calculated C-O bond of the extrinsic CO is much longer than that of free CO, which was calculated to be 1.15 Å. In fact, the calculated bond length of the extrinsic CO is rather similar to that of the calculated intrinsic CO, although for the former the experimental vibrational frequencies indicates a bond length intermediate between that of free and intrinsic CO.[4] As expected, a bridging CO has an even longer calculated C-O bond than a terminal CO. Therefore, none of the models satisfy the experimental results. Close examination of Table 2 reveals that both carbonyl ligands respond sensitively to changes of the overall charge of the active site.

Comparison of the experimental results of this work with the computational study done with ADF program precludes strong bonding of extrinsic CO to either metallic atoms of the active site. Recent nickel L-edge soft X-ray spectroscopy experiments [47] and recent theoretical calculations [48] support the existence of high-spin Ni(II) in the active site of the reduced and CO-inhibited states. Therefore, we have done calculations using Gaussian program for a model of weakly bound **SI-CO** with high-spin Ni(II) (Figure 8). For comparison, the calculated analytical frequencies for **SI** and **SI-CO** and the experimental ones are listed in Figure 8. The constancy of the differences between the experimental and theoretical values supports this structure as a suitable model for **SI-CO**.

Discussion

D. fructosovorans hydrogenase is highly homologous to the *D. gigas* hydrogenase [49]. In addition, both enzymes have similar EPR properties [14, 15] and their crystallographic structures are also quite alike, especially in the active site [6, 7, 50, 51]. Therefore, it is not surprising that their IR characterization gives very similar results with only slight differences between frequency values (Table 1). The differences between the IR spectra of both enzymes and those reported for *Chromatium vinosum* are also slight [8]. It seems that the basic structure of the active site is the same for most of Ni-Fe hydrogenases and that their catalytic mechanism is also similar. Therefore, experimental results obtained on the structure or function of one of these hydrogenases can be easily compared with those reported in the literature for others.

In this work we have obtained direct evidence by IR-spectroelectrochemistry that the hydrogenase states **A**, **B**, **SU** and **R** are stable in the presence of CO, whereas **SI** and **C** evolve to species which have extrinsic CO bound to the active site. Binding of CO to the hydrogenase active site is thought to be favored in the more electron-rich states as the CO binds to metals predominantly as an π-acceptor. In fact, the chemistry of Ni model compounds shows that CO binding is favored in the more reduced Ni states [52]. This can explain why **A** and **B** states do not bind extrinsic CO as they are generally considered as Ni(III) redox states [3, 4, 14, 19, 46, 53, 54]. **SU** and **SI** are probably Ni(II) states [46, 53, 55, 56] but only **SI** ligates extrinsic CO. Surely, CO-binding requires also access of the CO molecule to the active site metals. The access could be blocked by the oxygen ligand that bridges both metals in the **A** state [7]. It has been proposed that the activation process, thus the conversion from **SU** to **SI,** involves the loss of a bridging ligand [11, 57]. The experimental data obtained in this work are in line with this interpretation of the activation process. In addition, a recent X-ray absorption spectroscopic study reveals that upon conversion of **SU** to **SI** the short Ni-O bond is lost and the Ni site changes from five-

coordinate to four-coordinate [53]. Therefore, both FTIR and X-ray absorption spectroscopy are in agreement in this respect.

The IR spectrum of the **SI-CO** state of *D. fructosovorans* hydrogenases is very similar to the one reported for the equivalent species in *C. vinosum* hydrogenase [23]. The isotopic shift observed with ^{13}CO permits to identify unambiguously the band due to the stretching vibration of the extrinsic bound CO in both hydrogenases. In addition, we have detected a new CO-inhibited state by IR spectroscopy, which we have named **(SI-CO)$_{red}$**. Both CO-inhibited states are in redox equilibrium, as redox conversion between the two states is reversible and fits well to an one-electron Nernstian process. Initially, we thought that the redox process involved was the reduction of Ni(II) to Ni(I), and that the latter state corresponded to the EPR signal reported in the literature for CO-inhibited NiFe-hydrogenases [14, 22, 58]. However, the UV/visible and EPR measurements indicate that the redox process involved is the reduction of the proximal 4Fe4S cluster and that the reduction of the Ni atom of the active site beyond the Ni(II) state is not favored. In fact, the formal redox potential measured from the titration of the FTIR spectra of the CO-inhibited states (-325 mV) is very similar to the reported value for the redox titration of the EPR signal of the proximal 4Fe4S cluster of the enzyme at pH 8 (-340 mV) [51]. This means that the the redox state of the proximal [4Fe4S] cluster affects the electron density distribution at the active site, although it is 6 Å away [6], and that FTIR spectroscopy is sensitive enough to detect these subtle differences.

Oxidation of **SI-CO** to **B** by redox mediators is blocked. At +250 mV the FTIR spectra of **SI-CO** does not change (not shown), whereas the formal redox couple of the **B**/**SI** couple is –150 mV at pH 8.0 [11]. The probable reason is that the bound extrinsic CO makes unfavorable the oxidation of the active site to Ni(III) as CO is a strong π-acceptor ligand. Stoichiometric reduction of **(SI-CO)$_{red}$** to **R** is also blocked. A small proportion of **R** is formed upon reduction at redox potentials lower than -500 mV. We believe it is due to the

replacement of the bound CO by H_2 in some of the enzyme's molecules. This H_2 could be produced by the activity of a small number of hydrogenase molecules, which have not been inhibited by CO, in presence of methyl viologen reduced at the electrode. In fact, when an overpotential of –1 V was applied at the gold electrode, at which H_2 discharge takes place at the electrode surface [59], the conversion of **(SI-CO)$_{red}$** to **R** increased (not shown).

We have mentioned in the results section that protonation/deprotonation of **SI-CO** is blocked. Therefore, it seems that CO-inhibition of all hydrogenase activities is due to the fact that binding of this ligand impedes both electron and H^+ transfer at the active site.

The frequency value of the IR band due to the extrinsic bound CO in **SI-CO** and **(SI-CO)$_{red}$** practically excludes the possibility of a CO-bridging ligand between the two metals of the active site [52]. Accordingly, the C-O bond of the extrinsic carbonyl ligand in the CO-bridged models is computed much too long, and is clearly longer than in the isoelectronic models with CO terminally bound to Ni (Table 2). Binding of the extrinsic CO to the Fe metal as a terminal ligand is also excluded for the following reasons: a) vibrational coupling with the intrinsic CO ligand is not observed, whereas in CO-inhibited Fe-only hydrogenases it is observed [60]; b) the crystallographic structure of NiFe hydrogenases indicates that an arginine residue impedes by steric hindrance the terminal binding of extrinsic CO to the Fe [6, 7, 30] and this is confirmed by our calculations; c) data from EPR [61], EXAFS [53] and X-ray diffraction [62] spectroscopy favor binding of extrinsic CO to the Ni atom. However, none of the models with the additional CO terminally and strongly bound to Ni are consistent with the experimental results: none give short bond distances for the extrinsic CO (see Table 2), although a proximity of Ni and CO must be deduced from the hyperfine splitting observed in an EPR spectrum of hydrogenase inhibited with ^{13}CO [61]. Since the experimental frequency of the extrinsic CO is only 114 cm^{-1} lower than that of CO in solution and 125 cm^{-1} higher than that of the intrinsic CO, we conclude that the protein backbone prevents strong binding of extrinsic CO to the Ni atom. In consequence, only a weak interaction takes place.

In fact, the extrinsic CO ligand can be removed from the active site by replacing the CO atmosphere of the sample with H_2, whereas the intrinsic diatomic ligands are not exchangeable [23].The weak interaction of extrinsic CO to the active site would explain the smaller shift observed for its FTIR band upon reduction of the [4Fe4S] cluster compared to the intrinsic CO. Still, the binding of extrinsic CO to the active site is strong enough to block electron and H^+ transfer at the active site.

Figure 9 shows the mechanism we propose for CO-inhibition of NiFe hydrogenases. We represent form **C** as a Ni(III)-Fe(II) state with a bridging hydride and form **SI** as a Ni(II)-Fe(II) state with no bridging ligand because these structures have been proposed by several authors [45, 53, 56, 58]. We propose that binding of extrinsic CO to form **C** displaces H_2 from the active site and stabilizes the Ni(II) state. Controlled low redox potential of the sample causes reduction of the proximal 4Fe4S cluster via the distal 4Fe4S cluster, thus the **(SI-CO)$_{red}$** spectrum is observed. This is agreement with the results reported by Happe *et al.* of the binding of CO to *Chromatium vinosum* hydrogenase followed by EPR spectroscopy [58]. Rapid mixing/rapid freezing studies showed that the **C** state in presence of CO evolved quickly to an EPR-silent state. The EPR state **C-CO** could be only observed at 200 K after photo-dissociation of form **C** in the presence of CO [58]. As our FTIR experiments have been done at 298 K, we do not detect the **C-CO** state in this work.

Since our computational models does not take in account the protein backbone, they can not give detailed information about the structures of **C-CO** and **SI-CO,** but it can discard unreasonable structures and provide a first glimpse of a possible structural model for **SI-CO** as high-spin Ni(II) with a weakly coordinated CO. We plan, however, to use a hybrid QM/MM method for future studies that combines quantum mechanics (DFT in this case) and molecular mechanics [63]. This will allow including in the calculation parts of the protein backbone and thus allow better comparison with preliminary crystallographic data of CO-inhibited NiFe hydrogenase [62].

Acknowledgements. The Spanish Ministry of Science and Technology (project BQU2000-0991) and the European Union BIOTECH program (grant BIO-98-0280) supported this work. We thank Prof. Siem Albracht for useful discussions, Dr. Arturo Martinez-Arias for doing the EPR measurements, the Autonomous Community of Madrid (CAM) for the postdoctoral fellowship of A. L. De Lacey and the German Academic Exchange Service (DAAD) for the postdoctoral fellowship of C. Stadler. MBH thanks NSF (CHE-9800184) for financial support.

Supplementary material. Figure S1, containing the FTIR spectra of the potentiometric titration of the **SI-CO/(SI-CO)$_{red}$** couple, is available in electronic form on Spriger Verlag's server at http://link.springer.de/journals/jbic/

Footnotes

[1]The experiment was done in an outward laboratory and the glovebox was placed in a fume cupboard with forced ventilation and with a CO sensor. The operator weared a CO gas mask.

[2]Although the shift of three of the bands is smaller than the spectral resolution, it was reproducibly observed in all experiments.

[3]This was done to avoid interference of the redox dyes in the visible spectra. The same redox states of the hydrogenase can be detected in the spectroelectrochemical cell with and without redox dyes, although in the former case redox equilibrium is reached faster.

[4]The experimental IR frequency of the extrinsic CO is intermediate between the value of free CO in solution (2155 cm^{-1}) and the value of the experimental frequency of the intrinsic CO.

References

1. Adams MWW (1990) Biochim Biophys Acta 1020 : 115-145

2. Cammack R, Fernandez VM, Schneider K (1988) In: Lancaster JR, Jr. (ed) The Bioinorganic Chemistry of Nickel. VCH Publishers, Inc., New York, pp 167-190
3. Moura JJG, Texeira M, Moura I, LeGall J (1988) In: Lancaster JR, Jr. (ed) The Bioinorganic Chemistry of Nickel. VCH Publishers, Inc., New York, pp 191-226
4. Albracht SPJ (1994) Biochim Biophys Acta 1188 : 167-204
5. Thauer RK, Klein AR, Hartmann GC (1996) Chem Rev 96 : 3031-3042
6. Volbeda A, Charon MH, Piras C, Hatchikian EC, Frey M, Fontecilla-Camps JC (1995) Nature 373 : 580-58
7. Volbeda A, Garcin E, Piras C, De Lacey AL, Fernandez VM, Hatchikian EC, Frey M, Fontecilla-Camps JC (1996) J Am Chem Soc 118 : 12989-12996
8. Bagley KA, Duin EC, Roseboom W, Albracht SPJ, Woodruff WH (1995) Biochemistry 34 : 5527-5535
9. Happe RP, Roseboom W, Pierik AJ, Albracht SPJ, Bagley KA (1997) Nature 385 : 126
10. Pierik AJ, Roseboom W, Happe RP, Bagley KA, Albracht SPJ (1999) J Biol Chem 274 : 3331-3337
11. De Lacey AL, Hatchikian EC, Volbeda A, Frey M, Fontecilla-Camps JC, Fernandez VM (1997) J Am Chem Soc 119 : 7181-7189
12. Moura JJG, Moura I, Huyhn BH, Kruger HJ, Teixeira M, DuVarney RC, DerVartanian DV, Peck HD Jr, LeGall J (1982) Biochem Biophys Res Commun 108 : 1388-1393
13. Van der Zwaan JW, Albracht SPJ, Fontjin RD, Slater EC (1985) FEBS Lett 179 : 271-276
14. Cammack R, Patil DS, Hatchikian EC, Fernandez VM (1987) Biochim Biophys Acta 912 : 98-109
15. Hatchikian EC, Traore AS, Fernandez VM, Cammack R (1990) Eur J Biochem 187 : 635-643
16. Bagyinka C, Whitehead JP, Maroney M J (1993) J Am Chem Soc 115 : 3576-3585
17. Fernandez VM, Hatchikian EC, Cammack, R (1985) Biochim Biophys Acta 832 : 69-79

18. Roberts LM, Lindhal PA (1994) Biochemistry 33 : 14339-14349
19. Dole F, Fournel A, Magro V, Hatchikian EC, Bertrand P, Guigliarelli B (1997) Biochemistry 36 : 7847-7854
20. Hallahan DL, Fernandez VM, Hatchikian EC, Hall DO (1986) Biochimie 68 : 49-54
21. Fauque G, Peck HD Jr, Moura JJG, Huynh BH, Berlier Y, DerVartanian DV, Teixeira M, Przybyla AE, Lespinat PA, Moura I, LeGall J (1988) FEMS Microbiol Rev 54 : 299-344
22. Van der Zwaan JW, Albracht SPJ, Fontijn RD, Roelofs YBM (1986) Biochim Biophys Acta 872 : 208-215
23. Bagley KA, Van Garderen CJ, Chen M, Duin EC, Albracht SPJ, Woodruff WH (1994) Biochemistry 33 : 9229-9236
24. Montet Y (1998) Ph D. Thesis, Grenoble, France
25. Moss D, Nabedryk E, Breton J, Mäntele W (1990) Eur J Biochem 187 : 565-572
26. ADF 1999.02 and ADF 2000.02
27. FonsecaGuerra C, Snijders JG, Te Velde G, Baerends EJ (1998) Theor Chem Acc 99 : 391-403
28. Van Lenthe E, Snijders JG, Baerends EJ (1996) J Chem Phys 105 : 6505-6516
29. Van Lenthe E, Ehlers A, Baerends EJ (1999) J Chem Phys 110 : 8943-8953
30. Vosko SH, Wilk L, Nusair M (1980) Can J Phys 58 : 1200-1211
31. Frisch M J, Trucks G W, Schlegel HB, Scuseria GE, Robb MA, Cheeseman JR, Zakrzewski VG, Montgomery JA Jr, Stratmann RE, Burant JC, Dapprich S, Millam JM, Daniels AD, Kudin KN, Strain MC, Farkas O, Tomasi J, Barone V, Cossi M, Cammi R, Mennucci B, Pomelli C, Adamo C, Clifford S, Ochterski J, Petersson GA, Ayala PY, Cui Q, Morokuma K, Malick DK, Rabuck AD, Raghavachari K, Foresman JB, Cioslowski J, Ortiz JV, Baboul AG, Stefanov BB, Liu G, Liashenko A, Piskorz P, Komaromi I, Gomperts R, Martin RL, Fox DJ, Keith T, Al-Laham MA, Peng CY, Nanayakkara A, Gonzalez C, Challacombe M, Gill PMW, Johnson B, Chen W, Wong MW, Andres JL,

Gonzalez C, Head-Gordon M, Replogle ES, Pople JA (1998) GAUSSIAN 98, Revision A6; Gaussian, Inc., Pittsburgh, PA

32. Becke AD (1993) J Chem Phys 98 : 5648-5652
33. Lee C, Yang W, Parr RG (1988) Phy Rev B37 : 785-789
34. Hay PJ, Wadt WR (1985) J Chem Phys 82 : 270-283
35. Wadt WR, Hay PJ (1985) J Chem Phys 82 : 299-310
36. Couty M, Hall MB (1996) J Comput Chem 17 : 1359-1370
37. Ehlers AW, Böhme M, Dapprich S, Gobbi A, Höllwarth A, Jonas V, Köhler KF, Stegmann R, Veldkamp A, Frenking G (1993) Chem Phys Lett 208 : 111-114
38. LanL2dz: Dunning D95 basis sets on first row, Los Alamos ECP plus double- basis sets on Na-Bi
39. Höllwarth A, Böhme M, Dapprich S; Ehlers AW, Gobbi A, Jonas V, Köhler KF, Stegmann R, Veldkamp A, Frenking G (1993) Chem Phys Lett 208 : 237-240
40. Hariharan PC, Pople JA (1973) Theoret. Chimica Acta 28 : 213
41. Hehre WJ, Radom L, Schleyer PVR, Pople JA (1986) *ab initio molecular orbital theory*. Wiley, New York
42. Hehre WJ, Stewart RF, Pople JA (1969) J Chem Phys 51 : 2657
43. Banwell CN (1983) Fundamentals of Molecular Spectroscopy. McGraw-Hill Book Company, London
44. Niu S, Thomson LM, Hall MB (1999) J Am Chem Soc 121 : 4000-4007
45. Li S, Hall MB (2001) Inorg Chem 40 : 18-24
46. Stadler C, De Lacey AL, Volbeda A, Fontecilla-Camps JC, Conesa JC, Fernandez VM, manuscript in preparation
47. Wang H, Ralston CY, Patil DS, Jones RM, Gu W, Verhagen M, Adams M, Ge P, Riordan C, Marganian CA, Mascharak P, Kovacs J, Miller CG, Collins TJ, Brooker S, Croucher PD, Wang K, Stiefel EI, Cramer SP (2000) J. Am. Chem. Soc 122 : 10544-10552

48. Fan H-J, Hall MB (2001) J. Am. Chem. Soc (submitted)

49. Rousset M, Dermoun Z, Hatchikian EC, Belaich JP (1990) Gene 94 : 95-101

50. Montet Y, Amara P, Volbeda A, Vernede X, Hatchikian EC, Field MJ, Frey M, Fontecilla-Camps JC (1997) Nat Struct Biol 4 : 523-526

51. Rousset M, Montet Y, Guigliarelli B, Forget N, Asso M, Bertrand P, Fontecilla-Camps JC, Hatchikian EC (1998) Proc Nat Acad Sci USA 95 : 11625-11630

52. Nakamoto K (1997) Infrared and Raman Spectroscopy of Inorganic and Coordination Compounds. John Wiley & Sons, Inc., New York

53. Davidson G, Choudhury SB, Gu Z, Bose K, Roseboom W, Albracht SPJ, Maroney MJ (2000) Biochemistry 39 : 7468-7479

54. Trofanchuk O, Stein M, Geßner C, Lendzian F, Higuchi Y, Lubitz W (2000) J Biol Inorg Chem 5 : 36-44

55. Amara P, Volbeda A, Fontecilla-Camps JC, Field MJ (1999) J Am Chem Soc 121 : 4468-4477

56. De Gioia L, Fantucci P, Guigliarelli B, Bertrand P (1999) Inorg Chem 38 : 2658-2662

57. Higuchi Y, Ogata H, Miki K, Yasuoka N, Yagi T (1999) Structure 7 : 549-556

58. Happe RP, Roseboom W, Albracht SPJ (1999) Eur J Biochem 259 : 602-608

59. Katz E, De Lacey AL, Fierro JLG, Palacios JM, Fernandez VM (1993) J Electroanal Chem 358 : 247-259

60. De Lacey AL, Stadler C, Cavazza C, Hatchikian EC, Fernandez VM (2000) J Am Chem Soc 122 : 11232-11233

61. Van der Zwaan JW, Coremans JMCC, Bouwens ECM, Albracht SPJ (1990) Biochim Biophys Acta 1041 : 101-110

62. Higuchi Y (2000) Proceeding of the 6th International Conference on the Molecular Biology of Hydrogenases, Potsdam

63. Woo TK, Cavallo L, Ziegler T (1998) Theor Chem Acc 100 : 307-313

Figure Captions

- Figure 1: Redox states of Ni-Fe hydrogenases detected by FTIR.
- Figure 2: Model of the active site of *Desulfovibrio fructosovorans* hydrogenase used for the computational study with ADF program.
- Figure 3: A) Absolute IR spectra of 0.7 mM *D. fructosovorans* hydrogenase in 50 mM Tris buffer, pH 8.0, 100 mM KCl, in presence of redox mediators at different redox potentials: a) as isolated (resting potential was +229 mV), 2ºC, b) -280 mV, 2ºC, c) -245 mV, 25ºC, after activation (activation was achieved at -295 mV and 25ºC after 210 minutes), d) -395 mV, 25ºC, after activation, e) -495 mV, 25ºC, after activation f) +6 mV, 25ºC, after activation. B) The same as A) except that the enzyme solution had been saturated previously with CO.
- Figure 4: Potentiometric titration of the **SI-CO/(SI-CO)$_{red}$** couple: (filled circles) apparent integrated absorption intensity of the 1931 cm^{-1} band; (open circles) apparent integrated absorption intensity of the 1928 cm^{-1} band. Solid lines are the best-fit curves for a one-electron Nernstian process.
- Figure 5: IR spectra of 0.6 mM *D. fructosovorans* hydrogenase in 50 mM Tris buffer, pH 8.0, 100 mM KCl, in presence of redox mediators and saturated with CO at different redox potentials: A) Absolute spectrum after 180 minutes at -495 mV and 25ºC, B) Absolute spectrum after oxidation of A at –395 mV and 25ºC, C) Difference spectrum of B-A.
- Figure 6: IR spectra of 0.6 mM *D. fructosovorans* hydrogenase in 50 mM Tris buffer, pH 8.0, 100 mM KCl, in presence of redox mediators and saturated with ^{13}CO at different

redox potentials after activation: A) Absolute spectrum at -245 mV and 25ºC, B) Absolute spectrum at -395 mV and 25ºC, C) Difference spectrum of B-A.

- Figure 7: Visible difference spectra of 0.5 mM *D. fructosovorans* hydrogenase in 50 mM Tris buffer, pH 8.0, 100 mM KCl, saturated with CO and poised at different redox potentials: A) (–225 mV)-(0 mV), B) (-400 mV)-(-225 mV), C) (-500 mV)-(-400 mV).
- Figure 8: The DFT optimized geometry (Å) for SI-CO with high spin Ni(II).
- Figure 9: Proposed scheme of reaction of CO inhibitor with the **SI** and **C** states of Ni-Fe hydrogenases.

Table 1. IR frequencies (cm^{-1}) of the different active site redox states in *D. gigas* and *D. fructosovorans* hydrogenases.

redox state	*D. gigas*[a]	*D. fructosovorans*
A	1947, 2083, 2093	1947, 2084, 2096
B	1946, 2079, 2090	1946, 2080, 2091
SU	1950, 2089, 2099	1950, 2091, 2101
SI_I	1914, 2055, 2069	1913, 2054, 2069
SI_{II}	1934, 2075, 2086	1933, 2074, 2087
C	1952, 2073, 2086	1951, 2074, 2086
R_I	1940, 2060, 2073	1938, 2060, 2074
R_{II}	1923, 2050, 2060	1922, 2051, 2067

[a]Data obtained from reference [11]

Table 2. Calculated carbonyl bond lengths for various active site models with extrinsic CO

model structure				bond length (Å)	
oxidation state of Ni	protonation state of Cys66	bridging ligand	charge[a]	intrinsic C-O	extrinsic C-O
extrinsic CO bridging between Ni and Fe					
II	unprot	CO	-2	1.181	1.206
II	prot	CO	-1	1.208	1.200
extrinsic CO terminally bound to Ni					
III	unprot	–	-1	1.180	1.181
III	unprot	H^-	-2	1.188	1.189
II	unprot	–	-2	1.192	1.192
II	prot	–	-1	1.183	1.179
I	unprot	–	-3	1.201	1.199
I	prot	–	-2	1.193	1.198

[a] This is the overall charge of the dinuclear cluster consisting of the Ni atom the (uncharged) $Fe(CO)(CN)_2$ fragment and the four cysteine groups.

Figure 1

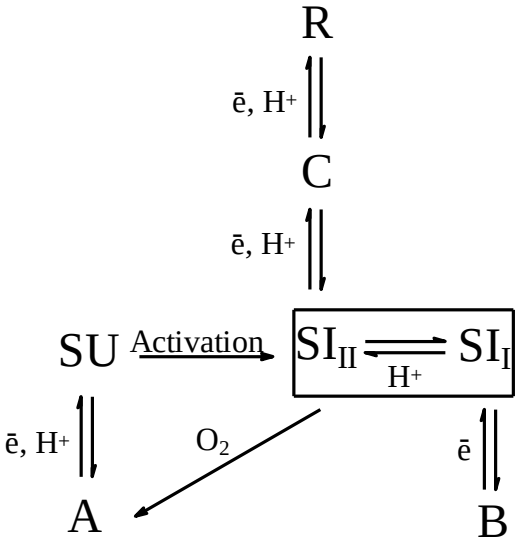

Figure 2

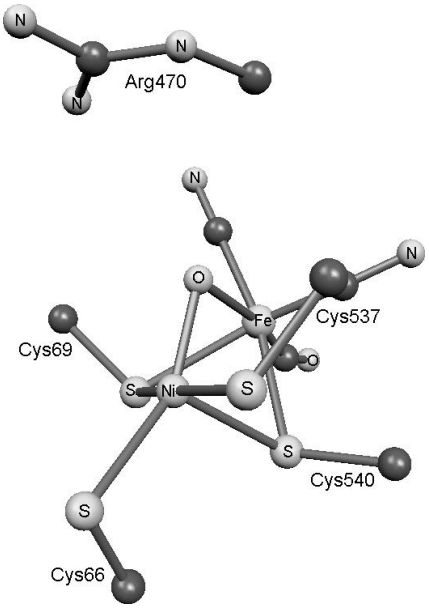

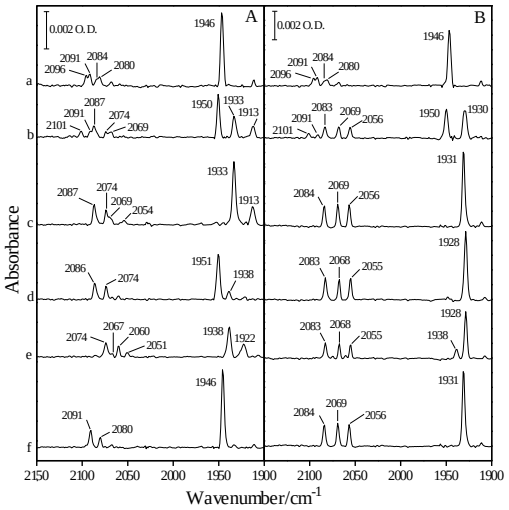

Figure 3

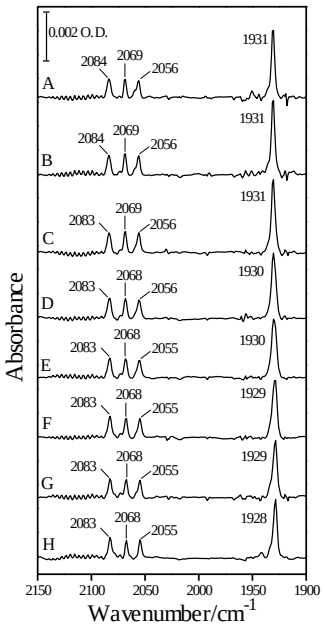

Figure 4

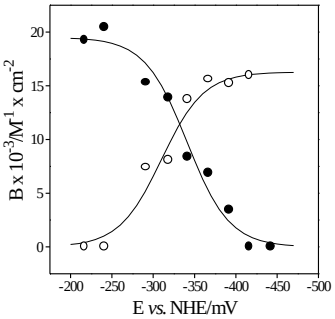

Figure 5

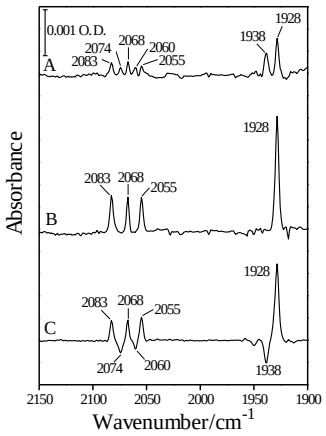

Figure 6

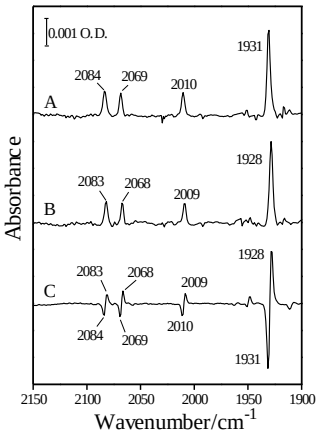

Figure 7

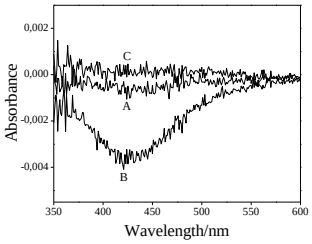

Figure 8

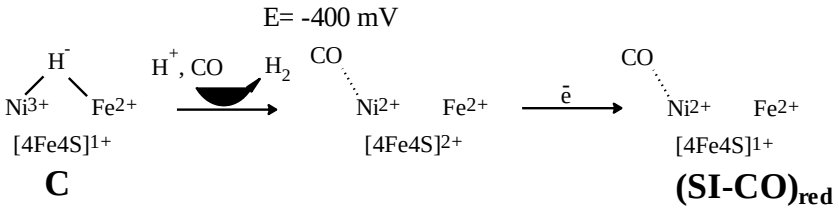

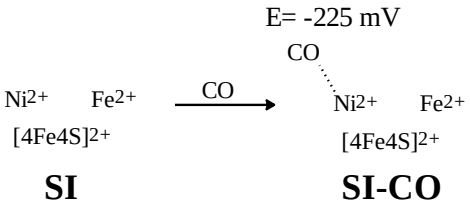

Figure 10

Supplementary material

- Figure S1: Absolute IR spectra of 0.8 mM *D. fructosovorans* hydrogenase in 50 mM Tris buffer, pH 8.0, 100 mM KCl, in presence of redox mediators and saturated with CO at different redox potentials after activation: A) -220 mV, B) -245 mV, C) -295 mV, D) -320 mV, E) -345 mV, F) –370mV, G) -395 mV, H) –420 mV. The temperature was 25ºC. The redox potentials were not applied in the sequence shown in the figure, they were imposed in the reduction and oxidation direction alternatively.